Shear-induced orientation of the body-centered-cubic phase in a diblock copolymer gel

I. W. Hamley* and J. A. Pople
School of Chemistry, University of Leeds, Leeds LS2 9JT, United Kingdom

C. Booth and L. Derici
Department of Chemistry, University of Manchester, Manchester M13 9PL, United Kingdom

M. Impéror-Clerc and P. Davidson
Laboratoire de Physique des Solides, Université Paris–Sud, Bâtiment 510, 91405 Orsay Cedex, France
(Received 6 July 1998)

The effect of steady shear on the alignment of a gel formed by block copolymer micelles in a body-centered-cubic (bcc) phase has been investigated using small-angle x-ray scattering (SAXS) for samples in a Couette cell. The gels were formed by an amphiphilic poly(oxyethylene)-poly(oxybutylene) diblock copolymer in an aqueous salt solution. The micellar hydrodynamic radius and mutual diffusion coefficient were obtained for solutions (micellar sols and gels) using dynamic light scattering. Static light scattering provided the micellar thermodynamic radius and association number. SAXS was used to probe the orientation of the bcc structure as a function of shear rate, and it was found that flow occurs with a [111] direction of the unit cell coincident with the shear direction, with twinning of the crystal about this axis. The SAXS experiments indicated a critical shear rate, $\dot{\gamma} \sim 50\ s^{-1}$ for macroscopic alignment of the gel. This value is lower than that reported in earlier publications from our group, where large-amplitude oscillatory shear was used to prepare highly oriented samples, possibly reflecting a dependence on strain amplitude. The viscoelastic behavior of the gel was probed using oscillatory shear and highly nonlinear rheology was observed at large strain amplitudes, which was assigned to a stick-slip mechanism of flow. The magnitude of the mutual diffusion coefficient, compared to the relaxation time obtained from the critical shear rate, also indicated a cooperative flow mechanism in the gel. [S1063-651X(98)07212-2]

PACS number(s): 61.25.Hq, 83.70.Hq, 61.10.−i, 83.50.Ax

I. INTRODUCTION

It is now firmly established that large-amplitude shear can be used to align ordered microstructures in block copolymer melts or gels in concentrated solutions [1]. For example, small angle neutron scattering has been used to examine the orientation of structures in block copolymer melts aligned by large-amplitude reciprocating shear in lamellar, [2,3] hexagonal [4,5] or body-centered-cubic (bcc) phases [6,7]. There has been particular interest in the shear conditions (shear rate and amplitude) required to obtain different orientations of the planes in the lamellar phase with respect to the shear direction [8]. The shear-induced alignment of ordered microstructures in concentrated block copolymer solutions has also been of recent interest. Of particular importance is the question of whether orientation increases continuously on varying shear conditions, or whether there are critical shear rates or amplitudes above which nonlinear flow leads to discontinuous changes in orientation. For example, steady shear applied to a solution of poly(styrene)-poly(isoprene) (PS-PI) in dioctyl phthalate above the equilibrium order-disorder transition was found to induce lamellar order above a critical shear rate, $\dot{\gamma} \sim 0.1\ s^{-1}$ [9], although such critical shear rates have not been reported for other ordered structures, such as the cubic micellar phases.

In this paper, we consider the effect of shear on orientation of the bcc phase formed in a concentrated solution of a diblock copolymer. The development of cubic order in such a block copolymer solution leads to the formation of a ''hard gel'' [10] which has a finite yield stress, and a typical dynamic elastic shear modulus $G' \sim 10^4$ Pa [11]. The formation of a gel phase was first reported to be correlated to the development of cubic ordering for a poly(styrene)-poly(butadiene) diblock copolymer in tetradecane [12,13]. Recent work supports this correlation between dynamic mechanical response and cubic micellar structure for aqueous solutions of Pluronic [poly(oxyethylene)-poly(oxypropylene)-poly(oxyethylene)] copolymers [10,14] and poly(oxyethylene)-poly(oxybutylene) diblocks [11]. Mortensen and co-workers [15–17] used shear to prepare aligned domains of Pluronic gels, the structure of which was elucidated using small-angle neutron scattering (SANS). In both $E_{25}P_{40}E_{25}$ (Pluronic P85) [15] and $E_{97}B_{39}E_{97}$ (Pluronic F88) [16,17], a bcc cubic phase was identified. The development of cubic ordering from a micellar solution in these and other Pluronic copolymers was interpreted in terms of a model of ''hard sphere crystallization'' [18,19]. However, hard sphere crystallization produces a cubic phase with a substantially lower hard sphere volume fraction, $\Phi = 0.494$ (for freezing of hard spheres) than bcc ($\Phi = 0.68$) or fcc ($\Phi = 0.74$) crystals. The effect of large-amplitude shear on face-centered-cubic structures has also been examined for Pluronic copolymers [20,21]. The effect of steady shear, applied using a Couette cell, on the orientation of a face-centered-cubic structure in $E_{127}P_{48}E_{127}$ (Pluronic F108) was

*Author to whom correspondence should be addressed.

investigated using small-angle x-ray scattering (SAXS), and transitions between different types of shearing flows were elucidated [20]. A twinned fcc structure with a high density of stacking faults due to flow of sliding layers was observed to transform into large homogeneous single crystals of either twin, separated on a millimeter scale, on application of large-amplitude oscillatory shear [21].

We have previously investigated the effect of large-amplitude shearing on cubic phases formed in concentrated solutions of diblock $E_{40}B_{10}$ in 0.2 M K_2SO_4, using SAXS with simultaneous rheology [22]. Salt was added to change the region of stability of the gel phase in the phase diagram, [23]. Both fcc and bcc phases were observed in this system depending on concentration (in the range 25–40 wt %) and temperature [22]. For polymer concentrations less than 30 wt %, only a fcc phase was observed. However, at higher concentrations, a bcc phase was observed at ambient temperatures, up to a transition to a high temperature fcc phase, the transition temperature increasing with polymer concentration. A hexagonal-packed rodlike micellar phase is formed in the same system at temperatures above about 75 °C, and we have also investigated the effect of large-amplitude shearing on the orientation of this structure [24]. Changes in the dynamic shear moduli upon application of large amplitude shear were compared to the global orientation of the system via simultaneous rheology and SAXS experiments.

In this paper, we first present results from dynamic and static light scattering experiments on copolymer $E_{86}B_{10}$ in 0.2 M K_2SO_4, where this salt solution was chosen to enable eventual comparison with other results for E_mB_n copolymers in the same series with constant B block length $n=10$ [22–29]. Dynamic light scattering provides the micellar hydrodynamic radius and the mutual diffusion coefficient, whereas static light scattering yields the thermodynamic radius and micellar association number. SAXS experiments on gels formed by this copolymer subjected to shear are then discussed. We have investigated systematically the extent of orientation on increasing the rate of steady shear, applied in a Couette cell by measuring SAXS patterns. We have previously reported simultaneous SAXS-rheology experiments on this system [25] and SANS measurements on gels subjected to steady shear, up to much higher shear rates than possible in the SAXS-rheology experiments [26]. In these papers, the mechanism for orientation of the bcc cubic phase was elucidated, and it was found that a [111] direction of the bcc structure aligns along the shear direction, with multiple twinning of (110) and (211) planes around this direction [25,26]. Here we present evidence for a critical shear rate for macroscopic alignment of the bcc gel. In addition, the nonlinear rheology of such a gel is investigated, and evidence for slip or slip-stick mechanisms of flow in the bcc lattice at large shear strain amplitudes is presented.

II. EXPERIMENT

A. Materials

The synthesis, by sequential anionic polymerization, and characterization of the diblock $E_{86}B_{10}$ has been described elsewhere [25]. It has a narrow molecular weight distribution, $M_w/M_n=1.04$ determined by gel permeative chromatography (GPC) based on poly(oxyethylene) calibrants. The materials used in the SAXS experiments were 35 wt % solutions of the copolymer in 0.2 mol dm^{-3} K_2SO_4 in H_2O or a 30 wt % solution in 0.2 mol dm^{-3} K_2SO_4 in D_2O. The latter was used to reduce incoherent scattering in previous small-angle neutron scattering experiments [26]. These solutions were prepared by mixing at $T=60-70$ °C, followed by several days storage in a refrigerator.

B. Light scattering

Static light scattering (SLS) intensities were measured by means of a Brookhaven BI-200SM instrument with vertically polarized incident light of wavelength $\lambda=488$ nm supplied by an argon-ion laser (Coherent Innova 90) operated at 500 mW or less. The intensity scale was calibrated against benzene. Measurements were made at a scattering angle $\theta=90°$. Dynamic light scattering (DLS) measurements were made under similar conditions by means of the instrument described above combined with a Brookhaven BI-9000AT digital correlator. Measurements of scattered light were made at an angle of 90° to the incident beam. Experiment duration was in the range 5–20 min, and each experiment was repeated two or more times. The applicability of these methods to micellar solutions of the type under investigation was discussed previously [30–32]. Glassware was washed with condensing acetone vapor before use. Solutions were clarified by filtering through Millipore Millex filters (triton free, 0.22-mm porosity, sometimes 0.1-mm porosity) directly into the cleaned scattering cell.

The correlation functions from DLS were analysed by the constrained regularized CONTIN method [33] to obtain distributions of decay rates (Γ). The decay rates gave distributions of apparent mutual diffusion coefficient [$D_{\rm app}=\Gamma/q^2$, $q=(4\pi n/\lambda)\sin(\theta)$, where n is the refractive index of the solvent, λ is the wavelength, and θ is half the scattering angle]. Thus the apparent hydrodynamic radius ($r_{h,\rm app}$, the radius of the hydrodynamically equivalent hard sphere corresponding to $D_{\rm app}$) could be obtained via the Stokes-Einstein equation

$$r_{h,\rm app}=kT/(6\pi\eta D_{\rm app}), \tag{1}$$

where k is the Boltzmann constant and η is the viscosity of the solvent at temperature T.

The basis for analysis of SLS was the Rayleigh-Gans-Debye equation in the form

$$I-I_s=K^*cM_w, \tag{2}$$

where I is intensity of light scattered from solution relative to that from benzene, I_s is the corresponding quantity for the solvent, c is the concentration (in g dm^{-3}), M_w is the mass-average molar mass of the solute, and

$$K^*=(4\pi^2/N_A\lambda^4)(n_B^2/R_B)(dn/dc)^2, \tag{3}$$

where N_A is Avogadro's constant, n_B and R_B are the refractive index and Rayleigh ratio of benzene, respectively, and dn/dc is the specific refractive index increment. Values of dn/dc and its temperature increment were taken from previous work [23], where the sources of other quantities necessary for the calculations were given. It is noted that the

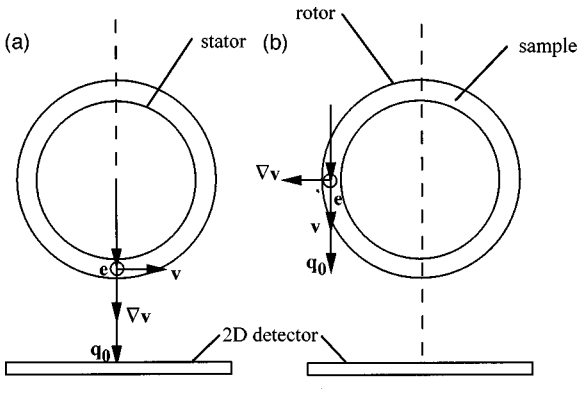

FIG. 1. Top view of the Couette cell showing the two geometries for the SAXS experiments. Here $\mathbf{v}$ is the velocity (shear) direction, $\nabla\mathbf{v}$ is the shear gradient direction, and $\mathbf{e}=\mathbf{v}\times\nabla\mathbf{v}$ is the neutral (vorticity) direction. (a) $(\mathbf{q}_v,\mathbf{q}_e)$ plane, (b) $(\mathbf{q}_\nabla,\mathbf{q}_e)$ plane.

refractive indices of poly(oxyethylene) and poly(oxybutylene) are very similar, making correction for refractive index difference unnecessary.

C. Small angle x-ray scattering

SAXS experiments at the European Synchrotron Radiation Facility (ESRF) were performed on the high brilliance beamline (BL4). Further details of this instrument are provided elsewhere [34]. Pinhole optics were employed to collimate a monochromatic incident x-ray beam (wavelength $\lambda=1$ Å) to a cross section 0.2×0.2 mm^2 at the sample position. The SAXS patterns were recorded on a two-dimensional gas detector in an evacuated tube. The detector was located 3 m from the sample. Samples were sheared in a homemade Couette cell, made of polycarbonate, that is described in detail elsewhere [35]. The rotor is the outer cylinder (the inner diameter of the rotor is 21 mm) and the size of the annular gap between both cylinders of the cell is 1 mm. The cell is mounted on a motorized translation stage which allows the sample to be aligned in any beam position between the so-called radial and tangential configurations (Fig. 1). Denoting the incident wave vector by $\mathbf{q}_0$ ($|q_0|=4\pi\sin\theta/\lambda$), the radial orientation corresponds to $\mathbf{q}_0$ parallel to $\nabla\mathbf{v}$, the velocity gradient direction. The tangential configuration corresponds to $\mathbf{q}_0$ parallel to $\mathbf{v}$, the shear velocity direction. The third direction $\mathbf{e}=\nabla\mathbf{v}\times\mathbf{v}$ is the vorticity direction. These two configurations provide the SAXS pattern in two orthogonal planes in reciprocal space, namely, $(\mathbf{q}_v,\mathbf{q}_e)$ and $(\mathbf{q}_\nabla,\mathbf{q}_e)$. The temperature of the Couette cell was controlled via a water bath, being stable to ±0.5 °C, following equilibration at the set temperature.

SAXS experiments were also performed at LURE (Laboratoire pour l'Utilisation du Rayonnement Électromagnétique), Orsay, France. Beamline *D*24 was used with an x-ray wavelength $\lambda=1.49$ Å, and a camera length of 2.5 m. Diffraction patterns were recorded using Fuji image plates, read on a molecular dynamics image plate scanner. Samples were sheared in a Couette cell similar to that used at the ESRF. This device is restricted to operation at room temperature.

D. Rheology experiments

Measurements of the dynamic elastic shear moduli were performed on a gel containing 32.5% $E_{86}B_{10}$ using a Rheometrics RSA II rheometer. The quantities G' (storage modulus) and G'' (loss modulus) are defined in the linear viscoelastic regime, where the stress is given by [36]

$$\sigma=G'A_0\sin(\omega t)+G''A_0\cos(\omega t) \tag{4}$$

for a sinusoidal (frequency ω) input strain of peak amplitude A_0

$$A=A_0\sin(\omega t). \tag{5}$$

In addition, nonlinear viscoelasticity was investigated as follows: The voltage output signal from the force transducer, providing a measure of the stress, was obtained along with the input strain wave form and captured using a LeCroy 9310A digital oscilloscope. The captured wave forms were also displayed as Lissajous figures of force versus applied strain.

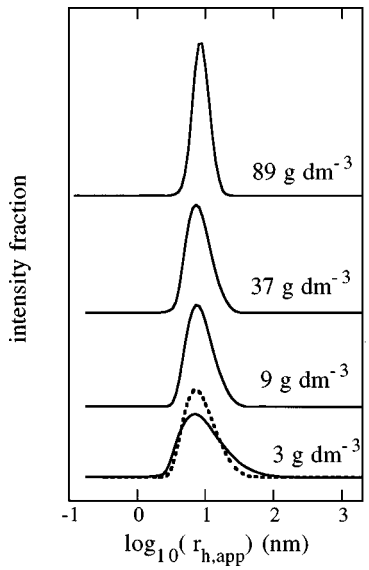

FIG. 2. Results from CONTIN analysis of DLS data for solutions of $E_{86}B_{10}$ at 20 °C at the concentrations indicated. The dotted line is data for the 3 g dm^{-3} solution at 45 °C.

III. RESULTS AND DISCUSSION

A. Dynamic light scattering

A measure of micellar size is provided by the hydrodynamic radius, extracted from DLS measurements on the gels. These measurements have the advantage that the micelle size is measured directly in the gel phase rather than in a dilute micellar solution. Results from DLS experiments for solutions of the copolymer in 0.2 M K_2SO_4 solution at 20 °C are shown in Fig. 2, where they are presented as plots of intensity fraction against the logarithm of the apparent hydrodynamic radius, $\log_{10}(r_{h,\mathrm{app}})$. The single peaks centered on $r_{h,\mathrm{app}}\approx80$ Å are characteristic of micelles in systems which undergo a closed association. The broad distribution found for the lowest concentrations used (3 g dm^{-3}) is typical of the response of the CONTIN analysis to a distribution affected by micellar dissociation. The dotted curve in Fig. 2 is the distribution found for the 3 g dm^{-3} solution at 45 °C. The narrowed distribution at this temperature, at which the solvent is poorer, is consistent with limited micellar dissocia-

TABLE I. Micellar characteristics from dynamic light scattering: copolymer $E_{86}B_{10}$ in 0.2 mol dm^{-3} aqueous K_2SO_4. Estimated uncertainties: D_{app} and r_h, ±5%; δ_h, ±15%.

T/°C	$D_{app}/10^{-11}$ m^2 s^{-1}	r_h/Å	δ_h
20	2.4	84	25
30	3.2	83	19
45	4.4	85	14

tion. The critical micelle concentration (CMC) at 25 °C will be less than 0.2 g dm^{-3}, based on a recent correlation between CMC and B block length for E_mB_n diblock copolymers in water [37], whereas the critical gel concentration (CGC) is at 16 wt % copolymer. The results in Fig. 2 confirm that the hydrodynamic radius does not vary on passing from a micellar sol to a gel.

As can be seen in Fig. 2, the peak position is not very sensitive to concentration, which is consistent with the salt solution being a poor solvent for the poly(oxyethylene) blocks. Accordingly, values of the micelle diffusion coefficient were equated with D_{app} measured at $c=9$ g dm^{-3}, i.e., a low concentration at which the copolymer was well micellized (see Fig. 2). These values are listed in Table I, together with values of r_h calculated from Eq. (1), and corresponding values of the hydrodynamic expansion factor ($\delta_h = \nu_h/\nu_a$,). The volume ν_h is the hydrodynamic volume calculated from r_h for spherical geometry, and ν_a is the anhydrous volume of a micelle calculated from the micelle molar mass (M_w; see Table II for results from static light scattering) and the copolymer density ($\rho \approx 1.10$ g cm^{-3}). As can be seen, the hydrodynamic radius is insensitive to temperature, an effect attributed many years ago [38] to compensation between an increase in association number (N_w) and a decrease in hydrodynamic expansion factor (δ_h) as temperature is increased and the solvent becomes poorer. It can be assumed that the former reduces draining of solvent through the micelle fringe, while the latter reduces the extension of the blocks in the fringe. The effect has been found for many other block copolyethers in aqueous solution [23,30,39].

B. Static light scattering

For a nonideal, dilute, solution of particles, the Debye equation can be written

$$K^*c/(I-I_s) = 1/M_w + 2A_2c\cdots, \tag{6}$$

where A_2 is the second virial coefficient (higher terms being omitted from Eq. (6). As written, the equation assumes small particles relative to the wavelength of the light. Radii of gyration estimated from the hydrodynamic radii of Table I, were ~80 Å; hence any effect of destructive interference on the Debye function calculated from scattering at 90° can be safely ignored.

TABLE II. Micellar characteristics from static light scattering: copolymer $E_{86}B_{10}$ in 0.2 mol dm^{-3} aqueous K_2SO_4. Estimated uncertainties: N_w, 15%; M_w and δ_t, ±10%; r_t, ±5%.

T/°C	$M_w/10^{-5}$ g mol^{-1}	N_w	δ_t	r_t/Å
20	0.65	14	3.5	43
30	0.85	18	3.5	47
45	1.25	27	3.2	52

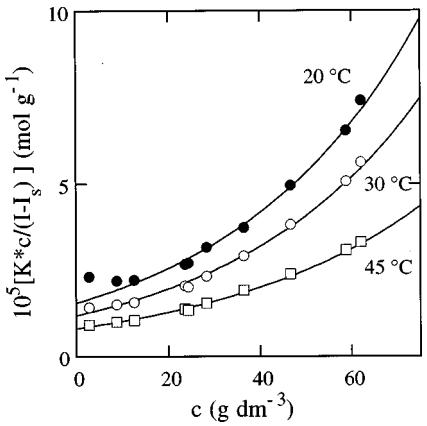

FIG. 3. Debye plot of the concentration dependence of static light scattering intensity (at 20 °C), following Eq. (6).

Use of Eq. (6), truncated to the second term, to measure the molar mass of the micelles is not satisfactory for the present system. There are two reasons: (i) micellar dissociation at low concentrations may cause an upturn in the Debye plot; and (ii) micellar interaction at moderate concentrations causes a curvature of the Debye plot across the whole concentration range. These features are illustrated in Fig. 3, the effect of micellar dissociation being small but clearly seen in the data for solutions at 20 °C. Given the curvature in the plots, the data were extrapolated to zero concentration from the moderate concentration range guided by the theory of scattering from uniform hard spheres [40], making use of the Carnahan-Starling equation [41]. Details of the procedure can be found elsewhere [23,30–32]. Fitting the data (as shown in Fig. 3) requires the density of the anhydrous copolymer and two adjustable parameters: the mass-average molar mass M_w and the thermodynamic expansion factor δ_t, defined as the ratio of the thermodynamic volume (ν_t, one eight of the excluded volume) to the anhydrous volume (ν_a): $\delta_\tau = \nu_t/\nu_a$. Values of M_w and δ_t are listed in Table II, together with association numbers of the micelles calculated from

$$N_w = M_w(\text{micelle})/M_w(\text{molecule}), \tag{7}$$

using a value of M_w(molecule) = 4700 g mol^{-1}. Also listed in Table II are values of the thermodynamic radius calculated from the thermodynamic volume (i.e., from $\nu_t = \delta_t\nu_a$).

C. Small-angle x-ray scattering

SAXS patterns in the ($\mathbf{q}_v$,$\mathbf{q}_e$) plane from a 35 wt % gel under shear at 25 °C are shown in Fig. 4. The diffraction patterns contain reflections in the positional ratio $1:\sqrt{2}:\sqrt{3}$. This is consistent with the bcc (space group $Im\bar{3}m$) structure observed for block copolymer melts and surfactant micellar solutions. The first order peak is centered on $q^* = 0.055$ Å^{-1}, close to the value previously reported for a 30 wt % gel of $E_{86}B_{10}$ in 0.2 M K_2SO_4 at 25 °C ($q^* = 0.056$ Å^{-1}) [26]. From this value of q^*, the bcc lattice

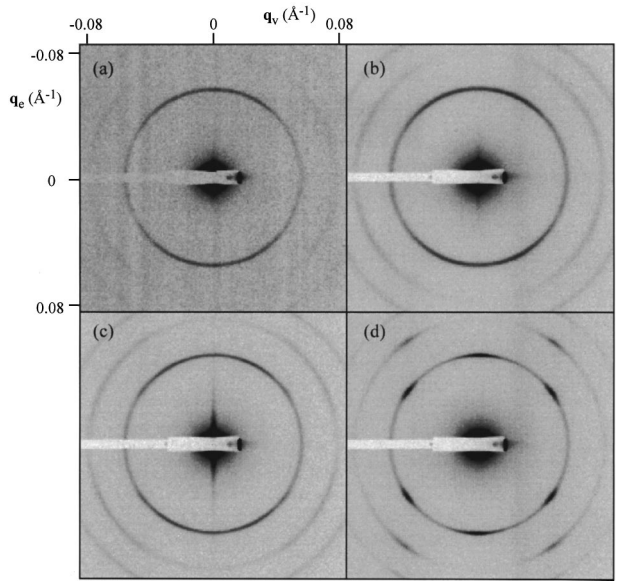

FIG. 4. SAXS patterns obtained in the $(\mathbf{q}_v, \mathbf{q}_e)$ plane while shearing a gel with 35 wt % $E_{86}B_{10}$ in 0.2 M K_2SO_4 ($T = 25$ °C) at shear rates $\dot{\gamma}/s^{-1}$=(a) 5, (b) 10, (c) 50, and (d) 100.

parameter is estimated as $a = 162$ Å [42]. Assuming a bcc packing fraction $\Phi = 0.68$ [43], this yields a micellar radius $R = 70$ Å [42], in good agreement with the hydrodynamic radii obtained from DLS and listed in Table I. Within the assumption of a uniform hard sphere structure, made in analyzing the SLS data, the radius of gyration in dilute solution is obtained as $r_g = \sqrt{3/5} r_h$ at 20 °C, in substantial agreement with the value for the gel. Correspondence between r_g (dilute solution) and R (gel) has been noted for other micellar systems [15–19]. As reported previously for other block copolymer systems in aqueous solutions (e.g., Refs. [23,44]), the thermodynamic expansion factor δ_t is a satisfactory predictor of the critical gel concentration. Using the value $\Phi = 0.68$, the critical volume fraction of copolymer for gel formation at 25 °C is $0.68/\delta_t = 0.19$, corresponding to 20 wt %. This compares with 16 wt % found in our laboratory for a related copolymer, nominally $E_{90}B_{10}$, in the same solvent, for which we find $\delta_t = 4.3$ by static light scattering. The basis of this prediction of the cgc is that δ_t is constant over a wide concentration range, but not necessarily r_t and M individually.

This leads to the following interesting observation for solutions and gels at a fixed temperature (25 °C). In the gels studied (35 wt % copolymer, gel density 1.035 g cm^{-3} based on volume additivity) the mass per unit cell (volume 4.25×10^6 Å^3) is 4.4×10^{-18} g, hence the mass per micelle (two micelles per unit cell) is 2.2×10^{-18} g, i.e., a micellar molar mass in the gel of 1.3×10^6 g mol^{-1}. The corresponding value in dilute solution is 0.75×10^5 g mol^{-1} (from static light scattering, see Table II), as increase in micellar mass of a factor of 17 or so. Such an increase of micellar mass on passing from micellar solution to gel has not, to our knowledge, previously been noted. It presumably reflects the flexibility of the system which is inherent in the dynamic equilibrium between micelles and molecules. As the mass of copolymer increases, the packing constraint on small micelles becomes too large, and the micelles increase in radius and mass.

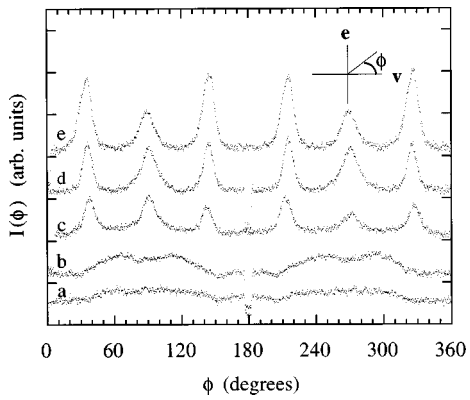

FIG. 5. Azimuthal intensity profiles obtained from SAXS patterns for the 35 wt % gel at 25 °C in the $(\mathbf{q}_v, \mathbf{q}_e)$ plane while shearing at shear rates $\dot{\gamma}/s^{-1}$=(a) 5, (b) 10, (c) 50, (d) 200, and (e) 500. Successive profiles have been shifted upwards for clarity. The break near $\phi = 180°$ results from the beamstop.

At low shear rates, the diffraction pattern exhibits a weak twofold anisotropy [Figs. 4(a) and 4(b)]. This is shown quantitatively by the azimuthal intensity profiles in Fig. 5. These were obtained by integration of the patterns in Fig. 5 in a narrow circular band centered on q^*. Patterns in Fig. 4 and profiles in Fig. 5 indicate that sharp Bragg peaks first develop at a shear rate $\dot{\gamma} \approx 50$ s^{-1}, and then continue to sharpen up to the highest shear rate accessed, $\dot{\gamma} = 500$ s^{-1}. In oscillatory shear, previous results from simultaneous SAXS-rheology experiments indicate that macroscopic alignment of a gel of $E_{86}B_{10}$ in 0.2 M K_2SO_4 (40 wt % polymer) occurred at a strain amplitude $A_0 = 100\%$ at a shear rate between $\dot{\gamma} = 1.6$ and 16 s^{-1}. The lower critical shear rate in this case may reflect either a different mechanism of alignment during oscillatory shear versus steady shear [however, the ultimate aligned structure has the same symmetry, at least for the projection accessed via SAXS patterns in the $(\mathbf{q}_v, \mathbf{q}_e)$ plane]. More likely, this simply reflects the higher susceptibility of more concentrated gels to shear, as discussed elsewhere [22,25]. The critical shear rate $\dot{\gamma} \approx 50$ s^{-1} corresponds to an associated relaxation time $\tau \sim 20$ ms, assuming a Deborah number $D_e = 1$.

Patterns with the same symmetries as shown in Fig. 4 have been discussed in detail elsewhere [25,26], and we merely outline here the indexing of the patterns to an aligned structure. At low shear rates, the patterns contain inner {110} reflections oriented along the meridian. This indicates that the {110} planes in this direction are predominantly oriented in the $(\mathbf{v}, \nabla\mathbf{v})$ plane, although the presence of significant intensity around the ring indicates that the sample is by no means a monodomain. This is also evident from the presence of {200} reflections centered on the equator [Figs. 4(a) and 4(b)], which are assigned to separate grains in which {200} planes are oriented in the $(\mathbf{v}, \mathbf{e})$ plane.

At higher shear rates, the pattern shown in Fig. 4(d) develops. As confirmed in Fig. 5(e), this comprises two meridional reflections, with four stronger reflections oriented at $\pm 55°$ with respect to the meridian. The change of macroscopic alignment of the sample evidenced by Figs. 4 and 5 was shown to be reversible. This is illustrated by the azimuthal intensity profiles shown in Fig. 6. Following shear at $\dot{\gamma} = 5$ s^{-1}, twofold anisotropy was restored, and again, above

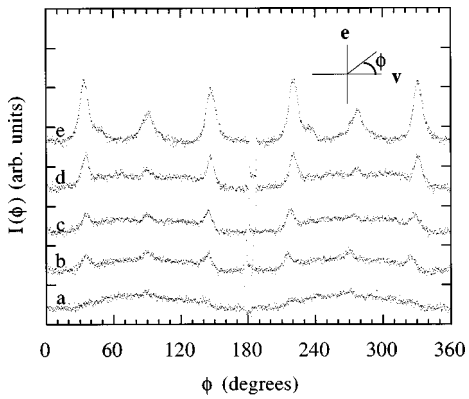

FIG. 6. Azimuthal intensity profiles obtained from SAXS patterns for the 35 wt % gel at 25 °C in the $(\mathbf{q}_v, \mathbf{q}_e)$ plane while shearing at shear rates $\dot{\gamma}/\mathrm{s}^{-1}$=(a) 5, (b) 50, (c) 100, (d) 200, and (e) 500 (second sequence of shear rate steps, cf plots for first sequence in Fig. 5). Successive profiles have been shifted upwards for clarity. The break near $\phi = 180°$ results from the beamstop.

a critical shear rate $\dot{\gamma} \approx 50\ \mathrm{s}^{-1}$, sharp Bragg reflections developed, with two on the meridian and four off-meridional reflections as obtained in the first sequence of shearing experiments.

In contrast to earlier work [25,26], shearing using a Couette cell enabled SAXS patterns to be obtained in two orthogonal planes, and representative patterns from the ''tangential configuration,'' i.e., the $(\mathbf{q}_\nabla, \mathbf{q}_e)$ plane, are shown in Fig. 7. At low shear rates, this indicates weak fourfold symmetry, at least of the {200} reflections, as apparent in Fig. 7(a), resulting from slip of these planes in the $(\mathbf{v}, \nabla\mathbf{v})$ and $(\mathbf{v}, \mathbf{e})$ planes. At shear rates above the critical value, sixfold symmetry is apparent, as shown by the pattern in Fig. 7(b). The evidence provided by the Couette cell shearing experiments on the symmetry of patterns in the $(\mathbf{q}_\nabla, \mathbf{q}_e)$ plane leads to an interpretation of the diffraction patterns from the aligned gel that is subtly different to that previously reported [25,26]. As in these earlier reports, the [111] direction of the bcc phase orients along the shear direction, and a twinned crystal is produced. The patterns from the current steady shearing experiments indicate that the shear direction is a sixfold symmetry axis, whereas it was previously identified as a threefold axis [25,26]. In the present case, diffraction patterns provide direct evidence for the symmetry in the $(\mathbf{q}_\nabla, \mathbf{q}_e)$ plane. Meanwhile, the patterns obtained above the

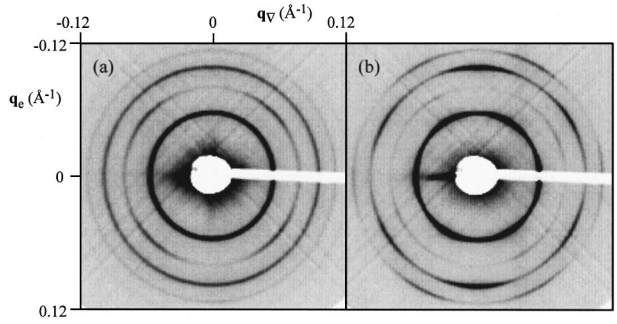

FIG. 7. SAXS patterns obtained patterns for the 35 wt % gel at 25 °C in the $(\mathbf{q}_\nabla, \mathbf{q}_e)$ plane while shearing at shear rates $\dot{\gamma}/\mathrm{s}^{-1}$=(a) 4 and (b) 800.

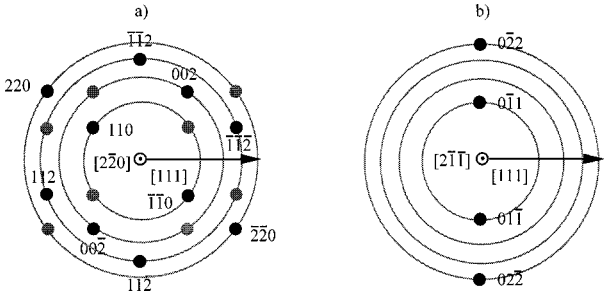

FIG. 8. Indexing of SAXS patterns in the $(\mathbf{q}_v, \mathbf{q}_e)$ plane obtained from the bcc phase oriented at high shear rates. The [111] direction is oriented along the shear direction. The patterns shown in Fig. 7 result from a superposition of patterns (a) and (b).

critical shear rate in the $(\mathbf{q}_v, \mathbf{q}_e)$ plane resemble those reported earlier, and are indexed on the basis of a twinned structure in Fig. 8. In particular, the twinning plane is perpendicular to (110)-type planes, and the twins are oriented at 35.3° with respect to the shear direction ([111]), being indicated by the 110 reflections at this angle with respect to the [111] direction in Fig. 8(a). This model also indicates that (110) planes are stacked along the shear gradient direction. This orientation of a bcc phase has been reported previously for a diblock copolymer copolymer melt oriented by reciprocating shear [6].

We now consider the nonlinear flows that lead to the macroscopic alignment of the bcc gel. Rheology experiments were conducted by applying oscillatory strain to a gel in the rheometer at $T = 20\ °\mathrm{C}$. Voltage signals corresponding to the input sinusoidal strain and the output transducer force (proportional to stress) were collected by a digital oscilloscope. Figure 9 presents representative results for a 33 wt % $E_{86}B_{10}$ gel subjected to shear at a frequency $\omega = 100\ \mathrm{rad\ s}^{-1}$. In this figure, the stress and strain wave forms are plotted for three periods of oscillation on the left-hand side, while Lissajous figures of the corresponding data are presented on the right-hand side. All plots are rescaled to give common axis ranges in each plot for force or strain. Viscoelastic behavior is exhibited at a strain amplitude $A_0 = 0.5\%$ (top), the force is essentially sinusoidal, and the Lissajous pattern is concentrated in one direction. In contrast, at strains as low as $A_0 = 2\%$, the force is out of phase with the input strain, and the Lissajous pattern is an elliptical shell. At $A_0 = 10\%$, the measured force becomes strongly nonsinusoidal, with higher harmonics apparent in the wave form. In the alternative Lissajous representation, the pattern becomes lozenge shaped (where we adopt the notation of Ref. [45]) with evidence of slip toward the extrema of the figures; i.e., at the largest strains the force is essentially independent of strain. Slip is even more dramatically illustrated at higher strains ($A_0 = 50\%$, bottom) where the force is independent of strain over a large part of the cycle. However, at the extrema of the Lissajous figures, the force (stress) becomes an increasing function of strain, corresponding to strain hardening. We refer to the resulting Lissajous figure as a ''bow-tie'' pattern. The combination of slip for part of a strain cycle, with strain hardening at the extremum of a cycle, suggests that a stick-slip mechanism operates at high strain amplitudes. Lozenge-shaped patterns were not obtained at lower frequencies ($\omega = 10\ \mathrm{rad\ s}^{-1}$) even at large strain amplitudes. In fact, the

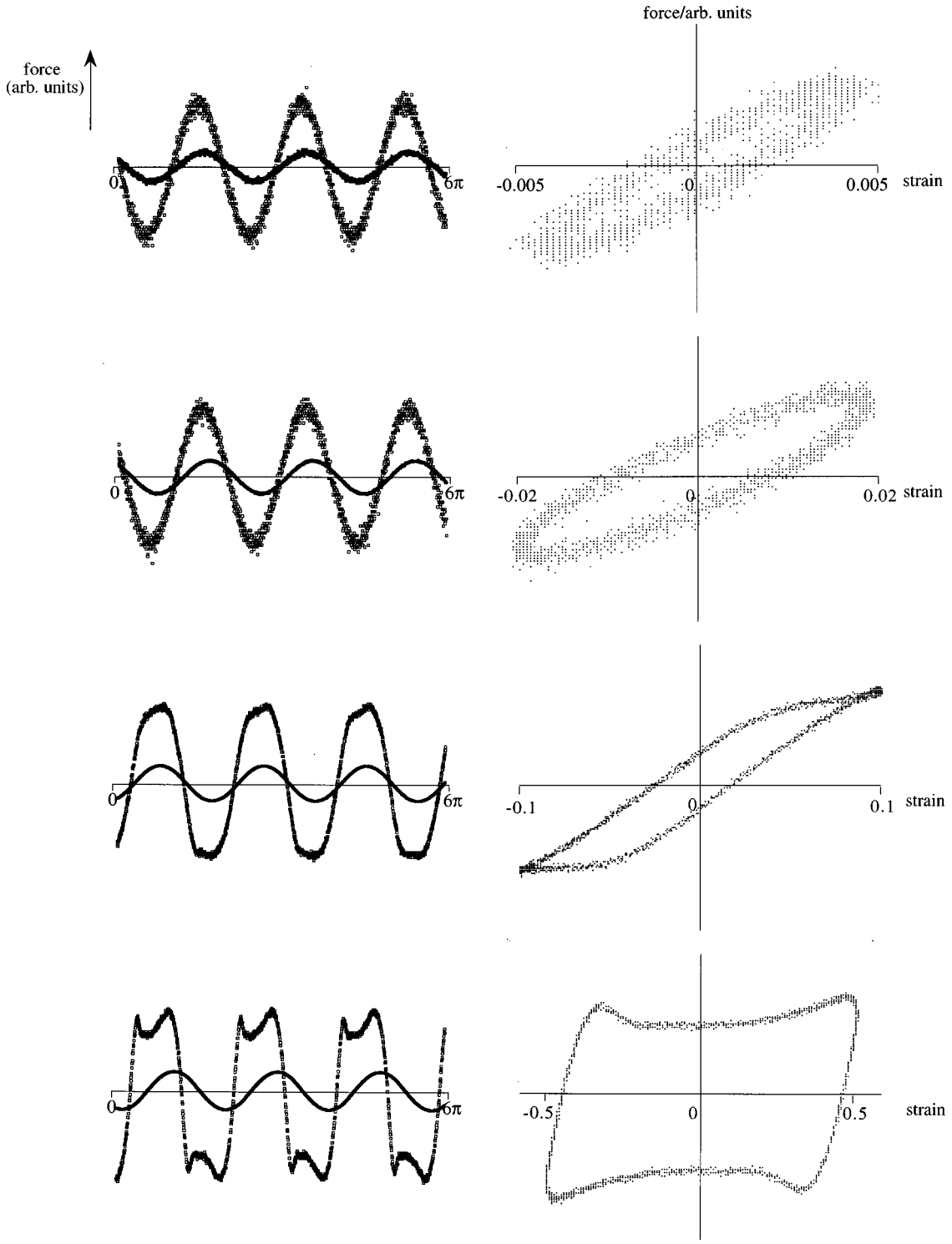

FIG. 9. Nonlinear viscoelasticity exhibited by a 33 wt % gel of $E_{86}B_{10}$ subjected to oscillatory strain deformation at $\omega = 100$ rad s^{-1} and indicated strain amplitudes A_0 ($T = 20$ °C). Left: voltage output by rheometer corresponding to applied strain (filled symbols) and measured force (open symbols). The ordinates have been rescaled to give a common scale for strain or stress in each plot. Right: the wave form data presented in the form of Lissajous figures.

observation of Lozenge-shaped Lissajous figures at $\omega = 100$ rad s^{-1} for large strain amplitudes corresponds to the condition for macroscopic alignment of the sample, as indicated by SAXS [25]. We thus tentatively associate the critical shear rate for macroscopic sample alignment with the onset of a slip-stick mechanism of flow in the cubic lattice, which based on SAXS experiments occurs in the (110) planes in the [111] direction.

We interpret our results based on the approach of Ref. [45], whose authors employed a lattice model to analyze the viscoelasticity of a (hexagonal) micellar phase formed by a block copolymer. They developed analytical theories that

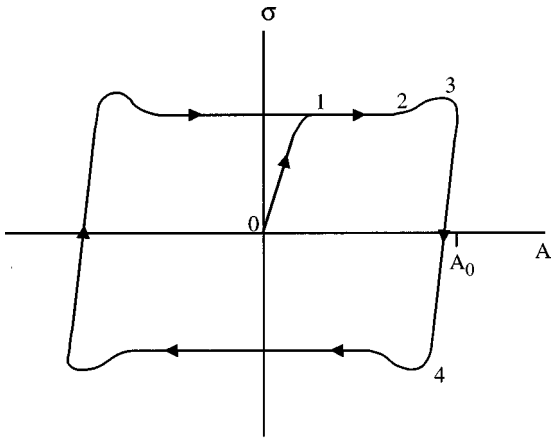

FIG. 10. Sketch of the ''bow-tie'' stress-strain pattern obtained for large amplitude shear strains, indicating the transient phase behavior (short times), and the resulting steady state cycle.

can describe complex Lissajous figures with strain softening features, or lozenge shapes at large strain amplitudes (whether these are obtained also depends on strain frequency). This theory was developed to account for the complex flows observed via cell dynamics simulations of the block copolymer hexagonal phase subjected to oscillatory strain deformation or to a step-strain deformation [46]. We expect that the essential physics of this two-dimensional lattice model will be applicable to three-dimensional cubic phases (because only two dimensions are relevant to shear flows). However, Ohta *et al.* [46] did not consider ''bow-tie'' patterns in their analytical model, although there is some evidence for their existence at large strain amplitudes in the cell dynamics simulations [46]. We focus on the bow-tie pattern obtained at the highest strain amplitude (Fig. 9, bottom), which can be interpreted on the basis of Fig. 10. During the transient development of stress (σ), initially all layers in the bcc lattice, within which flow occurs, start with approximately zero displacement (at the point labeled 0) and the strain amplitude $A=0$, the layers then follow the increasing strain. However, at the point indicated as 1 in the steady state cycle, slip commences and the force is independent of strain. This continues up to point 2, where the force (stress) begins to increase with strain, indicating strain hardening. This continues up to point 3, where the applied strain rate changes sign, at which point the stress follows the strain down to point 4, and so on for a complete cycle.

There have been few other experimental studies of nonlinear flows in block copolymer gels. Watanabe *et al.* [47] observed complex Lissajous figures obtained from measurements of the viscoelasticity of a PS-PI-PS triblock copolymer in a selective solvent. In addition, the nonsinusoidal stress response was described as a Fourier series, with expansion coefficients defining harmonic dynamic moduli. However, they were not able to correlate the nonlinear viscoelastic response of the gel to any specific flow behavior transitions, because structural characterization was not undertaken.

Based on our measured mutual diffusion coefficients (at infinite dilution) $D_{app}\sim 10^9$ Å^2 s^{-1}, the time taken to diffuse over one unit cell area is $\sim 10^{-5}$ s, which is two orders of magnitude smaller than the relaxation time associated with the critical shear rate $\tau\sim 20$ ms. From this we conclude that shearing above the critical shear rate leads to a structural relaxation which involves a large number of unit cells, and indeed this is consistent with the proposed stick-slip mechanism.

IV. SUMMARY

The effect of steady shear on the bcc phase formed by a poly(oxyethylene)-poly(oxybutylene) diblock copolymer in aqueous salt solution has been investigated using SAXS. Micellar dimensions were provided via static (micellar thermodynamic radius and association number) and dynamic (hydrodynamic radius and mutual diffusion coefficient) light scattering. The micelle mass in the gel is found to be much larger than that in the dilute state. In the SAXS experiments with *in situ* shearing in a Couette cell, a critical shear rate $\dot{\gamma}\sim 50$ s^{-1} for macroscopic alignment of the cubic phase was observed. This value is somewhat larger than that obtained in earlier experiments on the same system using oscillatory shear [25]. This is possibly due to the effect of strain amplitude, which is infinite for steady shear but finite for oscillatory shear. A detailed study was made of the effect of strain amplitude in oscillatory shear rheology experiments. The onset of nonlinear viscoelasticity was manifested in ''lozenge'' or ''bow-tie'' shaped Lissajous figures of stress as a function of strain. It is proposed that this results from a stick-slip mechanism of flow of lattice planes in the cubic structure.

ACKNOWLEDGMENTS

We are grateful to the EPSRC (U.K.) for Grant No. GR/K56117, which supported this work. We thank Dr. C. Bourgaux for assistance with the SAXS experiments at LURE and Dr. O. Diat for help in configuring the SAXS experiments at the ESRF. I. W. H., M. I.-C., and P. D. are grateful to the British Council for their financial support.

[1] I. W. Hamley, *The Physics of Block Copolymers* (Oxford University Press, Oxford, 1998), Chaps. 2 and 4.

[2] K. A. Koppi, M. Tirrell, F. S. Bates, K. Almdal, and R. H. Colby, J. Phys. II **2**, 1941 (1992).

[3] T. Tepe, D. A. Hajduk, M. A. Hillmyer, P. A. Weimann, M. Tirrell, F. S. Bates, K. Almdal, and K. Mortensen, J. Rheol. **41**, 1147 (1997).

[4] T. Tepe, M. F. Schulz, J. Zhao, M. Tirrell, F. S. Bates, K. Mortensen, and K. Almdal, Macromolecules **28**, 3008 (1995).

[5] K. Almdal, K. Mortensen, K. A. Koppi, M. Tirrell, and F. S. Bates, J. Phys. II **6**, 617 (1996).

[6] K. Almdal, K. A. Koppi, and F. S. Bates, Macromolecules **26**, 4058 (1993).

[7] K. A. Koppi, M. Tirrell, F. S. Bates, K. Almdal, and K.

Mortensen, J. Rheol. **38**, 999 (1994).
[8] Z.-R. Chen, J. A. Kornfield, S. D. Smith, J. T. Grothaus, and M. M. Satkowski, Science **277**, 1248 (1997), and references therein. Also see *The Physics of Block Copolymers* (Ref. [1]).
[9] N. P. Balsara, B. Hammouda, P. K. Kesani, S. V. Jonnalagada, and G. C. Straty, Macromolecules **27**, 2566 (1994).
[10] M. Almgren, W. Brown, and S. Hvidt, Colloid Polym. Sci. **273**, 2 (1995).
[11] C. Booth, G.-E. Yu, and V. M. Nace, in *Amphiphilic Block Copolymers: Self-Assembly and Applications*, edited by P. Alexandridis and B. Lindman (Elsevier, Amsterdam, 1998).
[12] H. Watanabe, T. Kotaka, T. Hashimoto, M. Shibayama, and H. Kawai, J. Rheol. **26**, 153 (1982).
[13] T. Hashimoto, M. Shibayama, H. Kawai, H. Watanabe, and T. Kotaka, Macromolecules **16**, 361 (1983).
[14] S. Hvidt, E. B. Jørgensen, W. Brown, and K. Schillén, J. Phys. Chem. **98**, 12 320 (1994).
[15] K. Mortensen, Europhys. Lett. **19**, 599 (1992).
[16] K. Mortensen, W. Brown, and B. Nordén, Phys. Rev. Lett. **68**, 2340 (1992).
[17] K. Mortensen, Prog. Colloid Polym. Sci. **91**, 69 (1993).
[18] K. Mortensen and J. S. Pedersen, Macromolecules **26**, 805 (1993).
[19] K. Mortensen and W. Brown, Macromolecules **26**, 4128 (1993).
[20] J.-F. Berret, F. Molino, G. Porte, O. Diat, and P. Lindner, J. Phys.: Condens. Matter **8**, 9513 (1996).
[21] O. Diat, G. Porte, and J.-F. Berret, Phys. Rev. B **54**, 14 869 (1996).
[22] J. A. Pople, I. W. Hamley, J. P. A. Fairclough, A. J. Ryan, G.-E. Yu, and C. Booth, Macromolecules **30**, 5721 (1997).
[23] N.-J. Deng, Y. Z. Luo, S. Tanodekaew, N. Bingham, D. Attwood, and C. Booth, J. Polym. Sci. Part B: Polym. Phys. **33**, 1085 (1995).
[24] J. A. Pople, I. W. Hamley, N. J. Terrill, J. P. A. Fairclough, A. J. Ryan, G.-E. Yu, and C. Booth, Polymer **39**, 4891 (1998).
[25] I. W. Hamley, J. A. Pople, J. P. A. Fairclough, A. J. Ryan, C. Booth, and Y.-W. Yang, Macromolecules **31**, 3906 (1998).
[26] I. W. Hamley, J. A. Pople, C. Booth, Y.-W. Yang, and S. King, Langmuir **14**, 3182 (1998).
[27] J. A. Pople, I. W. Hamley, J. P. A. Fairclough, A. J. Ryan, and C. Booth, Macromolecules **31**, 2952 (1998).
[28] I. W. Hamley, J. A. Pople, J. P. A. Fairclough, N. J. Terrill, A. J. Ryan, C. Booth, G.-E. Yu, O. Diat, K. Almdal, K. Mortensen, and M. Vigild, J. Chem. Phys. **108**, 6929 (1998).
[29] I. W. Hamley, J. A. Pople, and O. Diat, Colloid Polym. Sci. **276**, 446 (1998).
[30] Y.-W. Yang, N.-J. Deng, G.-E. Yu, Z.-K. Zhou, D. Attwood, and C. Booth, Langmuir **11**, 4703 (1995).
[31] Y.-W. Yang, Z. Yang, Z.-K. Zhou, D. Attwood, and C. Booth, Macromolecules **29**, 670 (1996).
[32] Z. Yang, Y.-W. Yang, Z.-K. Zhou, D. Attwood, and C. Booth, J. Chem. Soc., Faraday Trans. **92**, 257 (1996).
[33] S. W. Provencher, Makromol. Chem. **180**, 201 (1979).
[34] P. Bösecke, O. Diat, and B. Rasmussen, Rev. Sci. Instrum. **66**, 1636 (1995).
[35] O. Diat, D. Roux, and F. Nallet, J. Phys. II **3**, 1427 (1993).
[36] C. W. Macosko, *Rheology, Principles, Measurements and Applications* (VCH, New York, 1994).
[37] A. Kelarakis, V. Havredaki, G.-E. Yu, L. Derici, and C. Booth, Macromolecules **31**, 944 (1998).
[38] D. Attwood, J. H. Collett, and C. J. Tait, Int. J. Pharm. **26**, 25 (1985).
[39] B. Chu and Z.-K. Zhou, in *Nonionic Surfactants: Polyoxyalkylene Block Copolymers*, edited by V. M. Nace (Dekker, New York, 1996), Chap. 3.
[40] A. Vrij, J. Chem. Phys. **69**, 1742 (1978).
[41] N. F. Carnahan and K. E. Starling, J. Chem. Phys. **51**, 635 (1969).
[42] Incorrect values were calculated in Ref. [26].
[43] F. Scordari, in *Fundamentals of Crystallography*, edited by C. Giacovazzo (Oxford University Press, Oxford, 1992), Chap. 6.
[44] Y.-W. Yang, Z. Ali-Adib, N. B. McKeown, A. J. Ryan, D. Attwood, and C. Booth, Langmuir **13**, 1860 (1997).
[45] M. Doi, J. L. Harden, and T. Ohta, Macromolecules **26**, 4935 (1993).
[46] T. Ohta, Y. Enomoto, J. L. Harden, and M. Doi, Macromolecules **26**, 4928 (1993).
[47] H. Watanabe, T. Sato, K. Osaki, M.-L. Yao, and A. Yamagishi, Macromolecules **30**, 5877 (1997).